Polymer Degradation and Stability 244 (2026) 111850

Contents lists available at ScienceDirect

Polymer Degradation and Stability

journal homepage: www.journals.elsevier.com/polymer-degradation-and-stability

Enhancing flame retardancy and ultraviolet aging resistance of intumescent flame retardant polypropylene by incorporating cerium oxide

Jingqi Feng [a,1], Ruiping Wang [a,1], Jiaqi Geng [a], Siqi Huo [b,*], Zhiyong Zhang [a], Miaojun Xu [a,*], Mingyang Zhu [a], Bin Li [a,*]

[a] Heilongjiang Key Laboratory of Molecular Design and Preparation of Flame Retarded Materials, College of Chemistry, Chemical Engineering and Resource Utilization, Northeast Forestry University, Harbin 150040, China
[b] School of Engineering, Centre for Future Materials, University of Southern Queensland, Springfield 4300, Australia

ARTICLE INFO

Keywords:
Polyethylene
Cerium oxide
Intumescent flame retardant
Ultraviolet aging resistance
Flame retardancy

ABSTRACT

The flame-retardant modification of polypropylene (PP) often deteriorates its resistance to ultraviolet (UV) radiation, leading to severe degradation in both flame retardancy and mechanical properties during long-term service. To address this issue, cerium oxide (CeO_2) was incorporated into an intumescent flame retardant (IFR) system to achieve synergistic flame retardancy and enhance anti-UV performance. The resultant PP/IFR/CeO_2 achieved a UL-94 V-0 rating with a limiting oxygen index (LOI) of 32.7 % at a total loading of only 20 wt% IFR and CeO_2. After UV irradiation for 120 h, the surface of PP/IFR/CeO_2 remained smooth, with only shallow cracks, and its water contact angle was maintained at 64.5°. The carbonyl index increased merely to 1.45, indicating a markedly low degree of photo-oxidative aging. In addition, the tensile strength and elongation at break decreased by 9.4 % and 28.5%, respectively, which were significantly smaller reductions than those of PP/IFR. The results indicate that CeO_2 can effectively improve the anti-UV performance and flame retardancy of PP/IFR, providing a valuable foundation for developing durable, flame-retardant PP composites with improved anti-UV performance.

1. Introduction

PP dominates industrial polymers owing to its balanced mechanical properties, durability, and cost-effectiveness. Its primary applications span packaging, automotive components, technical textiles, and medical devices [1–3]. However, PP is highly flammable, releasing a large amount of heat during combustion and accompanied by severe molten dripping, which is prone to causing large-scale fires [4–6]. PP also exhibits inherent sensitivity to UV light due to the relatively low bond energy (approximately 380 kJ/mol) of the C-H bonds on its numerous tertiary carbon atoms. This characteristic renders these bonds susceptible to becoming initiation sites for free-radical oxidation chain reactions during aging, ultimately leading to chain scission and performance degradation [7–10]. Although introducing flame retardants can address the flammability issue of PP, the presence of flame retardants will further weaken the UV aging resistance of PP. Consequently, the long-term outdoor application of such flame-retardant PP materials remains challenging [11–13].

In recent years, IFR systems have been widely applied to enhance the flame retardancy of PP [14,15]. Among them, the most representative formulation is composed of ammonium polyphosphate (APP), pentaerythritol (PER) and melamine (MEL) [16,17]. Despite their widespread use, APP/PER/MEL system suffers from several inherent limitations, including poor water resistance, migration tendency, and the need for a high loading level (>30 wt%) to achieve satisfactory flame retardancy [18–20]. These issues significantly impair the mechanical properties of PP. To address these limitations, it is critical to develop high-efficiency APP/PER/MEL-derived systems to enhance flame retardant performance while minimizing adverse effects on material properties. In IFR systems, APP plays a crucial role by releasing phosphoric acid or polyphosphoric acid during thermal decomposition, which acts as a strong dehydrating agent to catalyze char formation, thereby serving as both acid and gas source [21–25]. Consequently, the rational selection of a charring-foaming agent (CFA) as the carbon source to cooperate with APP is key to developing an effective IFR system for PP [26–29].

In addition to flame retardancy, enhancing the UV aging resistance of

* Corresponding authors.
E-mail addresses: Siqi.Huo@unisq.edu.au (S. Huo), xumiaojun@nefu.edu.cn (M. Xu), libinzh62@163.com (B. Li).
[1] J. Feng and R. Wang contributed equally to this work and were listed as co-first authors.

https://doi.org/10.1016/j.polymdegradstab.2025.111850
Received 4 November 2025; Received in revised form 5 December 2025; Accepted 6 December 2025
Available online 7 December 2025

PP is equally important for its long-term outdoor applications. CeO_2, as a rare earth metal substance, possesses a wide band gap of approximately 3.1 eV, enabling it to effectively absorb UV light [30,31]. Moreover, CeO_2 can synergistically enhance the flame retardancy of IFR by catalyzing the formation of a dense and stable char layer during polymer pyrolysis [32–36]. Jose et al [37] introduced CeO_2 into ethylene-vinyl acetate (EVA)/magnesium hydroxide (MDH) composites, leading to significant enhancements in both mechanical properties and flame retardancy. Specifically, the peak heat release rate (pHRR) of the obtained EVA/MDH/CeO_2 composite decreased from 490.6 kW/m^2 for EVA/MDH to 354.4 kW/m^2, while the composite also exhibited well-preserved mechanical properties after UV aging. These results demonstrate that CeO_2 holds great potential to simultaneously enhance the flame retardancy and UV aging resistance of IFR-containing PP composites, but such a synergistic effect has not been reported previously.

Therefore, we developed flame-retardant PP composites with enhanced UV aging resistance by simultaneously incorporating APP/CFA and CeO_2. The resulting composites were systematically evaluated for their flame retardancy, UV aging resistance, mechanical properties, and thermal stability. In addition, the underlying mechanisms of anti-UV aging and flame retardancy were investigated through a series of complementary tests.

2. Experimental

2.1. Experimental materials

Ammonium polyphosphate (APP) was provided by Shandong Shian Chemical Co., Ltd., China. CFA (N-ethyl triazine-piperazine copolymer) was obtained from our laboratory [38]. Polypropylene (PP) was provided by Daqing Huake Co., Ltd., China. Cerium oxide (Micron-level) was provided by Suzhou Youyan Materials Co., Ltd., China. All materials were used as received.

2.2. Preparation of PP composites

PP, APP, CFA and CeO_2 were dried under vacuum at 80 °C for 6 h to remove moisture before use. Then, the IFR (APP and CFA) and CeO_2 were evenly mixed with a high-speed grinder for 3 min. Subsequently, PP and the above mixture were blended in a twin-screw extruder, and the temperature of apparatus from feed zone to die zone was fixed at 165, 175, 180, 180, and 175 °C, respectively. Finally, testing samples were prepared in an injection modeling machine at 180 °C. The formulations of PP samples are shown in Table 1.

Table 1
The formulations, LOI values and UL-94 ratings of PP samples.

Sample	Loading (wt %)	IFR/CeO_2 mass ratio	UL-94 (3.2 mm)			LOI (%)
			Rating	Dripping	t_1+t_2 (s)	
PP	0	-	NR	Yes	>50	18.7 ± 0.2
PP-1	20	100:0	V-2	Yes	3	29.6 ± 0.2
PP-2	23	100:0	V-0	No	3	31.9 ± 0.2
PP-3	20	99:1	V-0	No	9	31.9 ± 0.2
PP-4	20	97:3	V-0	No	8	32.4 ± 0.2
PP-5	20	95:5	V-0	No	6	32.7 ± 0.2
PP-6	20	93:7	V-2	Yes	11	30.5 ± 0.2
PP-7	19	95:5	V-2	Yes	17	30.5 ± 0.2
PP-8	1	0:100	NR	Yes	>50	19.3 ± 0.2

2.3. Characterization

Please refer to the Supporting Information for details.

3. Results and discussion

3.1. UV aging resistance

PP-5 (named as PP/IFR/CeO_2 in the following sections) showed the highest LOI value and UL-94 rating among all samples, and thus its UV aging resistance was investigated and compared with that of PP and PP/IFR (PP-1 in Table 1) samples by different tests.

3.1.1. Surface morphology and mechanical properties

PP undergoes progressive aging when exposed to prolonged UV irradiation, with the severity of degradation being reflected in surface morphological changes [39,40]. As presented in Fig. 1a, unaged PP and PP composites exhibited smooth surfaces initially. After 40 h of UV exposure, surface cracking and reduced transparency emerged in pure PP. Following 80 h of irradiation, PP samples showed widened and deepened cracks that proliferated into a pronounced network, conclusively evidencing severe photo-oxidative degradation of the materials.

For PP/IFR samples, with the increase of UV irradiation time, the surface colour gradually became yellow, and the cracks did not appear on the surface until 40 h. For PP/IFR/CeO_2 samples, the surface morphology evolved similarly to that of PP/IFR sample, but formation of cracks proceeded more slowly under UV irradiation, even though the number of cracks increased with irradiation time. Both the PP/IFR and PP/IFR/CeO_2 composites exhibited significantly reduced crack density and depth compared to pure PP. This morphological distinction indicates lower aging severity in these composites under identical UV exposure durations due to the UV-absorbing properties of the triazine rings in CFA and CeO_2. The above results are consistent with the observations in the scanning electron microscope (SEM) images (Fig. 1a). Fig. 1b shows the colour difference value (ΔE) of PP/IFR and PP/IFR/CeO_2 samples. The ΔE increase rate of PP/IFR sample was 10.6 % higher than that of PP/IFR/CeO_2 sample, further confirming that the presence of CeO_2 further improved the UV aging resistance of PP/IFR. For pure PP, due to its transparent color, the change value of the ΔE was relatively small. During the late stage of aging, PP material generated microcracks, holes, and micro-plastic particles on its surface, which enhanced light scattering, resulting in a more pronounced surface colour difference [41].

As depicted in Fig. S1, after 120 h of UV irradiation, the water contact angle values of pure PP, PP/IFR, and PP/IFR/CeO_2 were 40.6°, 49.3°, and 64.5°, respectively. This progressive increase in hydrophobicity was found to inversely correlate with surface oxidation severity, indicating the preferential oxidation of methylene groups to hydrophilic oxygen-containing functionalities on the surfaces of PP and PP/IFR samples [42]. This enhancement in the UV aging resistance imparted by CeO_2 is further demonstrated.

As shown in Fig. 1c and d, the incorporation of IFR reduced both tensile strength and elongation at break of PP/IFR sample. With the addition of CeO_2, both tensile strength and elongation at break were slightly improved, and the reductions in tensile strength and elongation at break after UV aging were the lowest among three samples. These results confirm that CeO_2 is able to absorb UV light, thereby providing further protection to the matrix against UV-induced damage, inhibiting breakage of the PP main chain, maximizing the preservation of mechanical properties, and consequently retarding the photoaging process.

3.1.2. Carbonyl index

When oxygen was present, the side-chain methylene groups in PP

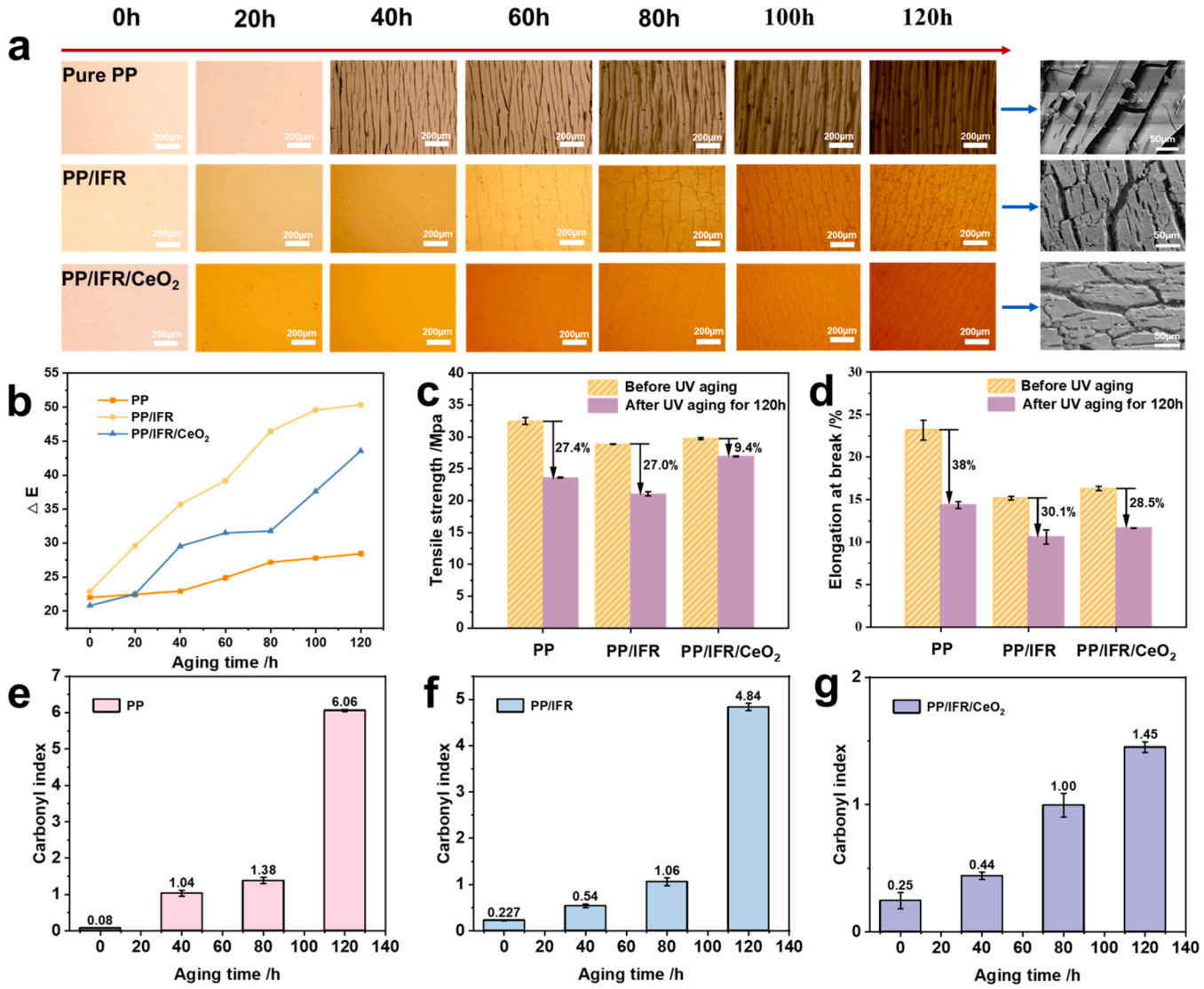

Fig. 1. Optical microscopy images of PP and PP composites after UV irradiation, with SEM images of PP and PP composites after 20 h of UV irradiation (a); The color difference values of PP and PP/IFR/CeO_2 after UV irradiation for different times (b); Tensile strength of PP and PP composites before and after 120 h of UV irradiation (c); Elongation at break of PP and PP composites before and after 120 h of UV irradiation (d); and Carbonyl index of PP and PP composites after UV irradiation for different times (e-g).

were oxidized to carbonyl groups under UV radiation, leading to main chain fracture and a shortened service life [43]. Therefore, the relative amount of carbonyl groups generated during photoaging was used as an indicator to evaluate the degree of photoaging for pure PP and its composites. The carbonyl index (CI) and carbonyl peak intensity at various photoaging durations for PP, PP/IFR, and PP/IFR/CeO_2 are presented in Fig. 1e-g and S2. PP showed a CI of 1.04 after 40 h of UV radiation, indicating the initiation of photo-oxidative degradation.

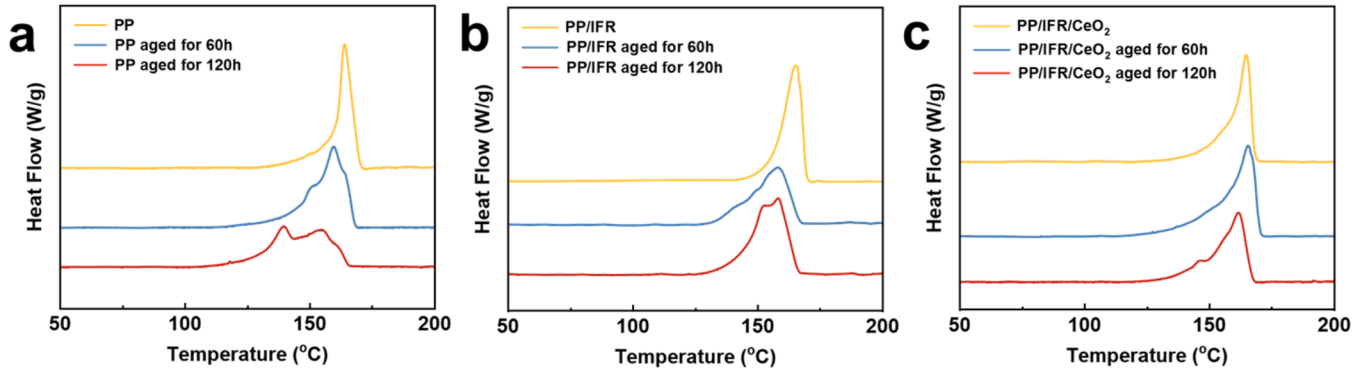

Fig. 2. Melting curves of PP (a), PP/IFR (b) and PP/IFR/CeO_2 (c).

Furthermore, the CI increased to 6.06 after 120 h of irradiation. PP underwent significant photo-oxidative degradation, which is consistent with the observations in Fig. 1a. The introduction of IFR delayed UV aging, leading to lower CI of PP/IFR than that of PP after 120 h of UV irradiation. Notably, the PP/IFR/CeO_2 showed the lowest CI, suggesting suppressed oxidation of side-methyl groups during photo-oxidative degradation. Thus, CeO_2 imparts superior UV-aging resistance to PP/IFR, thereby effectively delaying the aging process of PP [44].

3.1.3. Melting behaviors

Fig. 2 illustrated the variations in the melting behaviors of PP and PP composites before and after UV irradiation. Pure PP exhibited a single melting peak corresponding to α-type crystals at 164 °C (Fig. 2a). However, the melting peak temperature decreased with increasing aging time, and multiple melting peaks emerged after 60 h of aging. After 120 h of aging, the melting peaks associated with α-type crystals shifted to 155 °C, while those corresponding to β-type crystals shifted to 140 °C. This decrease was attributed to the oxidation of side methyl groups on the PP backbone to carbonyl ($C = O$) groups under UV irradiation, coupled with chain scission. These processes resulted in shorter polymer chains, which exhibited enhanced mobility during heating, thereby lowering the melting temperature. Consequently, the enhanced formation of β or γ-crystals during melting led to the appearance of multiple melting peaks.

The incorporation of IFR and CeO_2 affected the melting behaviors of PP. The melting temperatures (T_m) of PP/IFR and PP/IFR/CeO_2 samples were lower than that of pure PP. Both PP/IFR and PP/IFR/CeO_2 samples showed a single melting peak after 60 h of UV irradiation, but multiple peaks emerged after 120 h, indicating the enhanced UV aging resistance. After 120 h of aging, the T_m of PP/IFR sample belonging to α-crystals decreased to 159 °C and that corresponding to β-crystals reduced to 151 °C. The melting peaks of PP/IFR/CeO_2 sample showed relatively small changes, as shown in Fig. 2c. Thus, the presence of IFR and CeO_2 retarded the photoaging process, and fewer main chains of PP/IFR/CeO_2 were broken compared with pure PP under UV irradiation, thus the melting peak showed minimal change [31].

3.1.4. Mechanism of UV aging resistance

As depicted in Fig. S3, PP exhibited no distinct characteristic absorption peaks. In contrast, the incorporation of IFR and CeO_2 led to significant UV absorption peaks accompanied by reduced transmittance, confirming their superior UV absorption and shielding capabilities within the 250–350 nm range [45].

Fig. 3 illustrates the changes in the PP molecular chain and the formation of surface cracks in PP and PP composites during UV aging. With the increase of UV irradiation time, UV light could penetrate the material, resulting in the tertiary char structure of the PP main chain to be oxidised to form carbonyl groups. Meanwhile, the chemical bond broke, and the main chain started to fracture, leading to the reduced molecular weight and the emergence of surface cracks. With the addition of CeO_2, the electronic structure of CeO_2 consists of a valence electron band filled with electrons and a conduction band formed by empty orbitals without electrons. The energy gap between the valence band and conduction band, known as the forbidden band width (E), of CeO_2 is 3.1 eV. Under UV irradiation, the electrons in the valence band can be excited to the conduction band. Owing to its rich 4f electronic structure, CeO_2 can absorb UV light through electron excitation and subsequently release the absorbed energy as low-energy visible or infrared light and heat. This process effectively converts light energy into thermal or chemical energy, enabling CeO_2 to absorb UV radiation in the 200–400 nm range and thereby reduce the risk of polymer bond cleavage induced by UV exposure. In addition, CeO_2, which uniformly disperses within the PP matrix, can reduce UV light penetration by serving as a physical shielding. The triazine ring structure in the CFA molecule is also capable of absorbing UV energy [46]. Thus, both CFA and CeO_2 can effectively enhance the UV aging resistance of PP.

3.2. Thermal stability

Thermal stability of PP and its composites before and after UV aging were investigated *via* thermogravimetric (TG) analysis. The corresponding data, including temperature at 5% weight loss ($T_{5\%}$), temperature at maximum decomposition rate (T_{MAX}), maximum mass loss rate (R_{MAX}), and residual char yield at 800°C, are presented in Fig. 4 and Table S1. The incorporation of IFR and CeO_2 enhanced the thermal stability of PP, as evidenced by the increased $T_{5\%}$ relative to pure PP. Concurrently, the residual char yield at 800°C increased significantly from 0.73% of pure PP to 10.76% of PP/IFR and 11.70% of PP/IFR/CeO_2. These enhancements were attributed to the formation of intumescent char layers, which provided thermal insulation and retarded volatilization of degradation-derived small molecules [47–49]. As revealed in Fig. 4, the residual char of PP/IFR/CeO_2 at 800°C was lower than that of PP/IFR after aged for 120 h. The relatively poor UV-resistance of PP/IFR led to more significant scission of PP molecular chains and the viscosity of composites was declined, which contributed to the generation of expanded char layer. As a result, the residual char of PP/IFR was relatively higher than that of PP/IFR/CeO_2. After 120 h of UV aging, decreased $T_{5\%}$ and T_{MAX} values were observed for all PP

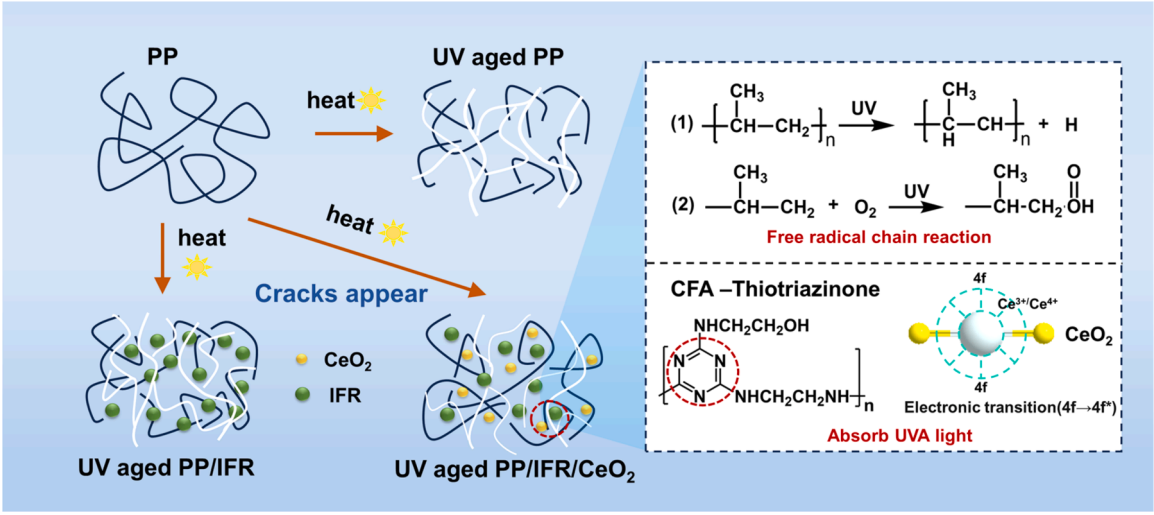

Fig. 3. Aging mechanisms of PP and PP/IFR/CeO_2.

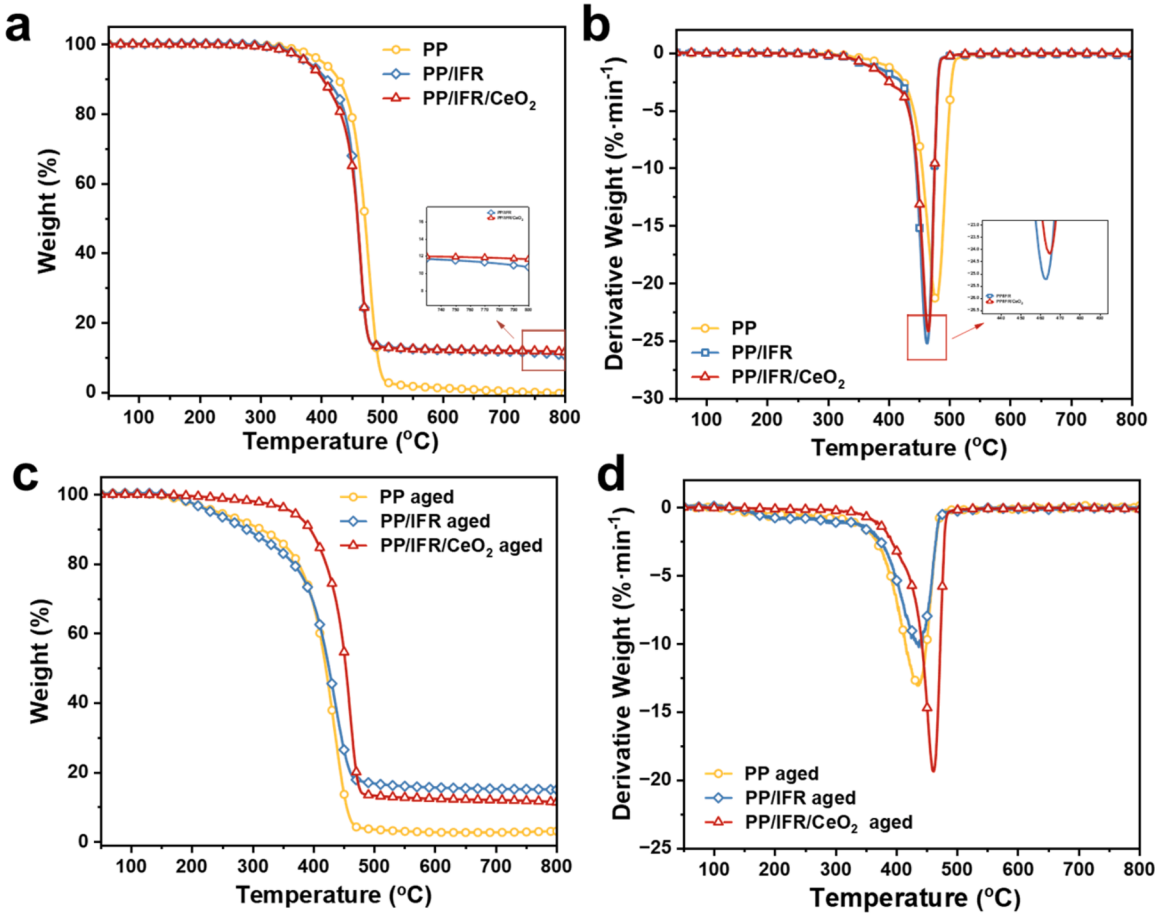

Fig. 4. TGA and derivative TG (DTG) curves of PP composite before (a, b) and after 120 h of UV aging (c, d).

samples, indicating accelerated decomposition. Compared with pure PP and PP/IFR, PP/IFR/CeO_2 showed smaller decreases in $T_{5\%}$ and T_{MAX}, further confirming the positive effect of CeO_2 on UV aging resistance.

3.3. Flame retardancy

3.3.1. LOI and UL-94 results

The LOI and UL-94 tests were applied to evaluate the flammability of PP and its composites, and the relevant data presented in Fig. S4 and Table 1. PP produced a lot of molten droplets during UL-94 test, and its LOI value was only 18.7 %, indicative of high flammability. Interestingly, when a small portion of IFR was replaced by CeO_2, the flame retardancy of PP composites increased markedly. Especially, the PP/IFR/CeO_2 presented the optimum flame retardancy with an LOI of 32.7 % when the mass ratio of IFR to CeO_2 was 95:5. In addition, it not only achieved V-0 rating in UL-94 tests but also quickly extinguished after two ignitions (Fig. 5c). As revealed in Table 1, there was no rating during vertical burning test for the PP/ CeO_2 sample with 1 wt% CeO_2, and the LOI was only 19.3 %. The fact indicated that only the addition of CeO_2 could not endow PP with good flame retardancy. Thus, there was a synergistic flame-retardant effect between CeO_2 and IFR.

3.3.2. Cone calorimetry results

The combustion behavior of PP and its composites was evaluated using cone calorimeter test (CCT), with corresponding data presented in Fig. 5d-g and Table 2. The time to ignition (TTI) of PP/IFR composite decreased from 21 s (pure PP) to 13 s. This reduction indicated promoted early degradation of the PP matrix by IFR. Furthermore, the TTI of PP/IFR/CeO_2 was further reduced to 11 s. As shown in Fig. 5d and e, pure PP exhibited a rapid increase in both heat release rate (HRR) and total heat release (THR) after ignition, with a pHRR of 1362.4 kW/m^2 occurring at 262 s. When 20wt % IFR was added, the HRR curve of PP/IFR showed two distinct peaks, with the first and second peak HRR values ($peak_1$—HRR and $peak_2$—HRR) reaching 506.7 and 518.5 kW/m^2, respectively. When 5wt % of IFR was replaced by CeO_2, the $peak_1$—HRR value of PP/IFR/CeO_2 decreased to 265.1 kW/m^2 and the $Peak_2$—HRR value reduced to 94.5 kW/m^2. In addition, the PP/IFR/CeO_2 sample had the lowest THR value of 65.1 MJ/m^2, which was 70.9 % and 66.7 % lower than those of pure PP and PP/IFR, respectively. Thus, the synergistic effect between IFR and CeO_2 endows PP with outstanding fire safety.

As depicted in Fig. 5f and g, pure PP exhibited a peak smoke production rate (pSPR) of 0.103 m^2/s. In contrast, the SPR curve of PP/IFR displayed two distinct peaks, with the first and second peak SPR values ($peak_1$-SPR and $peak_2$-SPR) of 0.040 and 0.080 m^2/s. The PP/IFR/CeO_2 composite similarly demonstrated two SPR peaks, with pSPR values of 0.017 and 0.012 m^2/s, which were reduced compared to those of PP/IFR. In addition, the total smoke production (TSP) decreased significantly from 17.6 m^2 (pure PP) and 20.2 m^2 (PP/IFR) to 5.7 m^2 for PP/IFR/CeO_2 (Fig. 5g). The enhanced smoke suppression of PP/IFR/CeO_2 was mainly due to the catalytic effect of CeO_2 on the formation of the carbonaceous, intumescent char layers during combustion. Such char barriers can trap smoke-generating hydrocarbons (e.g. alkanes, alkenes) within the condensed phase, thereby substantially suppressing smoke release.

3.3.3. Condensed phase analysis

Digital photographs of char residues from CCTs are presented in Fig. 6a-c. Complete combustion without any residual chars was observed for pure PP, whereas PP/IFR showed substantial intumescent char

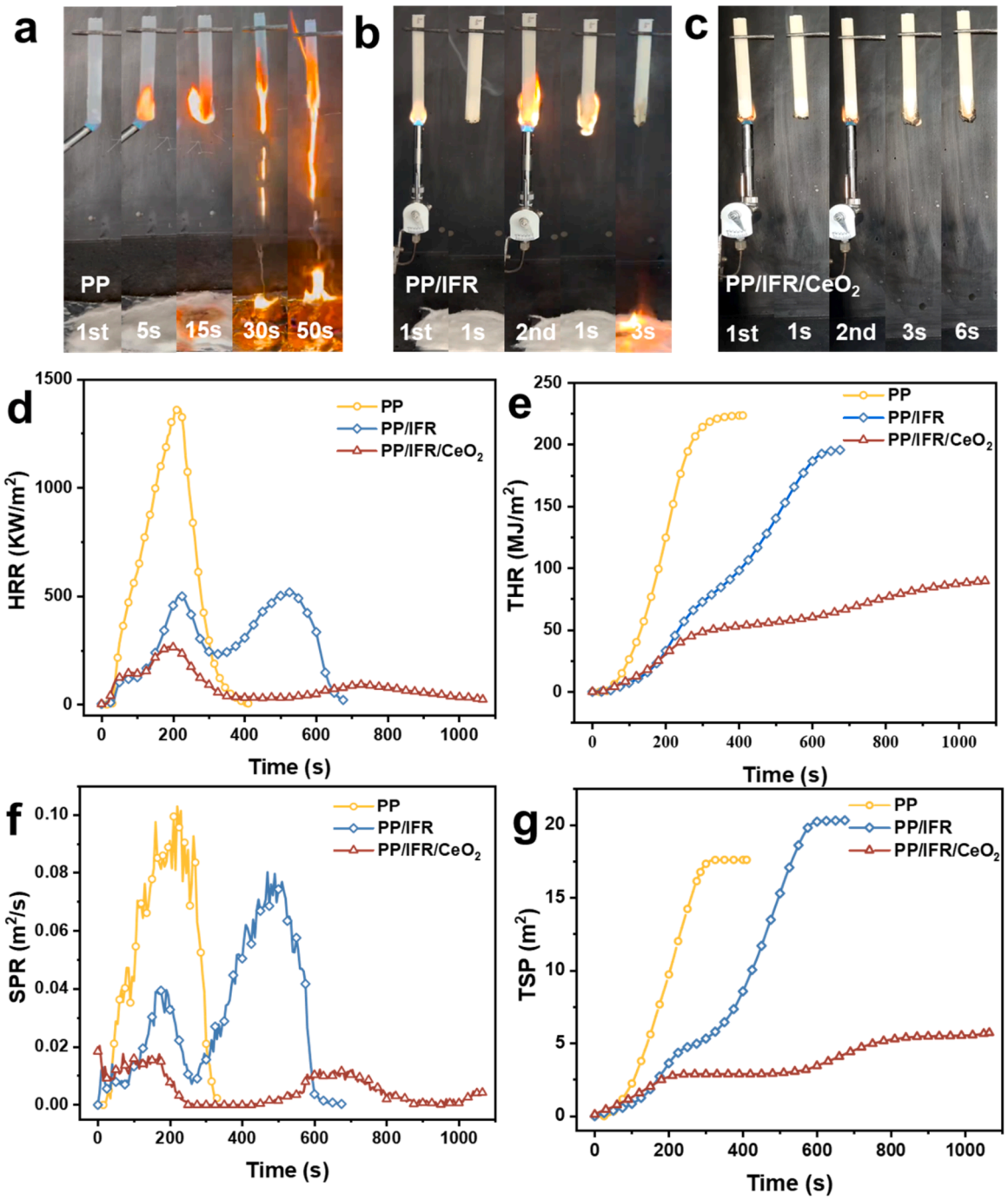

Fig. 5. Video screenshots of vertical combustion of pure PP (a), PP/IFR (b) and PP/IFR/CeO_2 (c); and HRR (d), THR (e), SPR (f), and TSP (g) curves of PP, PP/IFR and PP/IFR/CeO_2 samples.

Table 2
Cone calorimetry results of PP and its composite.

Sample	PP	PP/IFR	PP/IFR/CeO_2
TTI (s)	21±1	13±1	11±1
$peak_1$–HRR (kW/m^2)	1362.4 ± 16.3	506.7 ± 14.4	265.1 ± 11.9
$peak_2$–HRR (kW/m^2)	—	518.5 ± 9.0	94.5 ± 4.7
THR (MJ/m^2)	223.5 ± 7.9	195.6 ± 6.1	65.1 ± 3.2
$peak_1$-SPR (m^2/s)	0.103±0.009	0.040±0.007	0.017±0.002
$peak_2$-SPR (m^2/s)	—	0.080±0.001	0.012±0.001
TSP (m^2)	17.6 ± 1.2	20.2 ± 1.0	5.7 ± 0.5

formation. The introduction of CeO_2 significantly reinforced the char structure via catalytic carbonization. This intact barrier suppressed both heat and smoke during combustion. SEM images of char residues for PP composites were presented in Fig. 6d-g. Abundant wrinkles were observed within the residual char of PP/IFR, which partially hindered heat transfer and gas convection. However, further observation revealed the presence of perforations in the outer char wrinkles, mainly due to the loose structure of the intumescent char layer derived from IFR. During combustion, the released gases penetrated the char layer, and the propagation of cracks and the formation of pores undermined its structural integrity. Such degradation markedly reduced the thermal and oxidative barrier effectiveness of the char [50]. The incorporation of

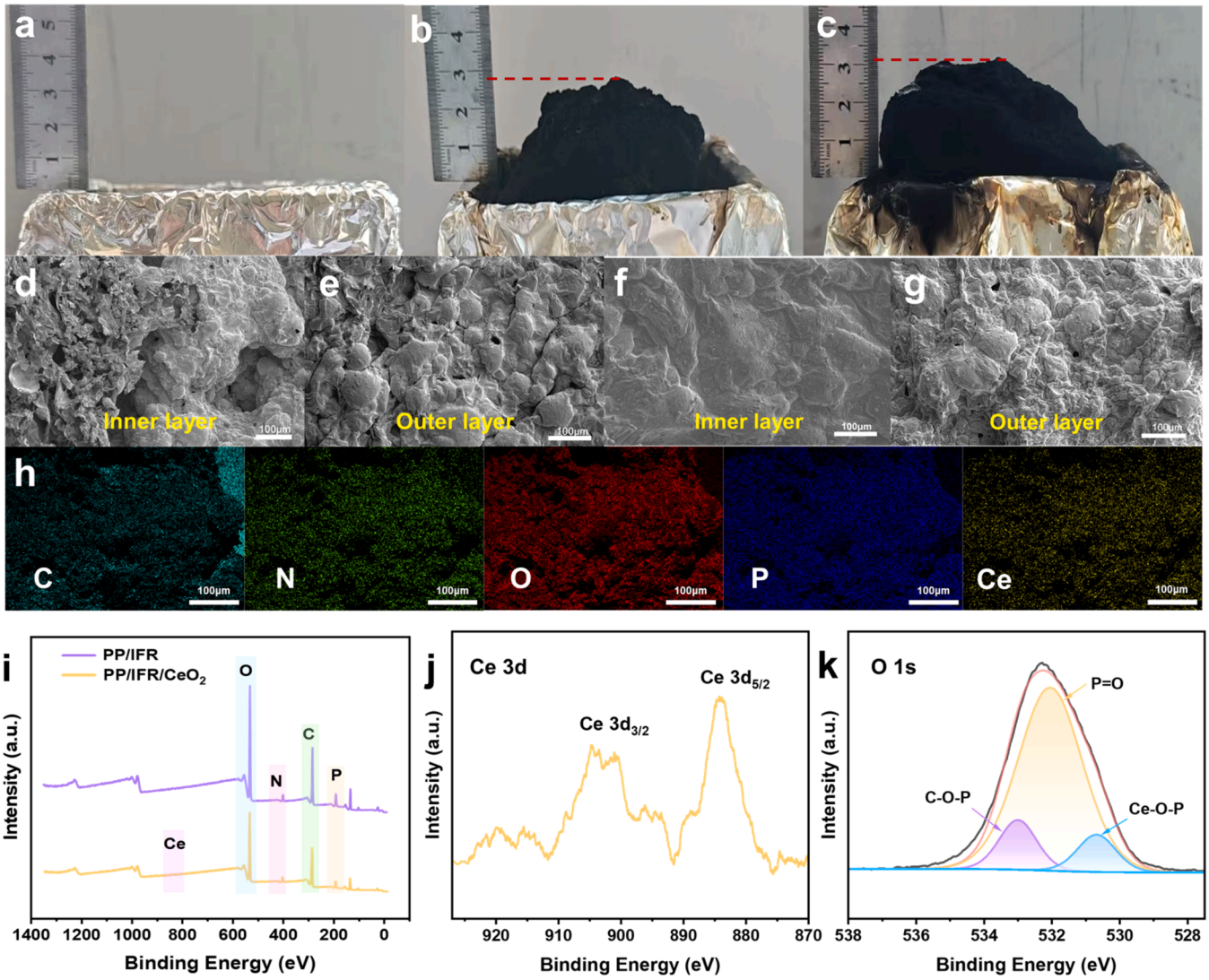

Fig. 6. The digital photos of char residues for PP (a), PP/IFR (b) and PP/IFR/CeO_2 (c); The SEM images of inner and outer char residues for PP/IFR (d, e) and PP/IFR/CeO_2 (f, g); The energy dispersive X-ray spectroscopy (EDS) mapping images of indoor char residue for PP/IFR/CeO_2 (h); The XPS full-scan spectra of PP/IFR and PP/IFR/CeO_2 chars (i); High-resolution XPS Ce 3D spectrum of PP/IFR/CeO_2 char (j); and The O 1 s spectrum of PP/IFR/CeO_2 char (k).

CeO_2 facilitated the formation of a denser char layer, where the enhanced wrinkles contributed to improved structural integrity. Elemental mapping in Fig. 6h identified C, N, O, P, and Ce within the indoor char layers of PP/IFR/CeO_2. Uniform elemental distribution was observed, effectively restricting heat/oxygen diffusion while suppressing smoke evolution and retarding flame propagation.

In order to further verify the chemical element composition of char layers for PP composites, the X-ray photoelectron spectroscopy (XPS) tests were performed, with the data listed in Fig. 6i-k and S5. Compared with PP/IFR char, the PP/IFR/CeO_2 char had two new peaks, which belonged to Ce $3d_{5/2}$ (882.3 eV) and Ce $3d_{5/2}$ (907 eV) bonds [51–53]. There were two peaks in the O1 s spectrum of PP/IFR, which were attributed to the $P = O$ (530.9 eV) and C—O-P (533.5 eV) bonds [54]. The appearance of the $P = O$ binding energy peak indicated the presence of phosphoric acid groups in the char layer, which promoted the dehydration and carbonization process. Except for the above two peaks, the PP/IFR/CeO_2 char showed a Ce-O-P peak at 530.5 eV, indicating that the Ce atom crosslinked with phosphate during combustion.

3.3.4. Gas phase analysis

The TG coupled with Fourier-transform infrared spectroscopy (TG-IR) tests of pure PP, PP/IFR and PP/IFR/CeO_2 were conducted to investigate the gas-phase flame-retardant mechanism (Fig. 7). Pure PP produced a large number of pyrolysis products such as alkanes (2964 cm^{-1}) and alkenes (1460 cm^{-1}). The gas decomposition products of PP/IFR were obviously reduced, and some inert gases such as NH_3 (965 cm^{-1}) were produced. Under heating, APP decomposed to produce phosphoric acid and metaphosphoric acid, which would promote the dehydration of polymers into carbon and isolate volatile alkanes in the char layer. Meanwhile, the decomposition of CFA produced NH_3 gas, and the formed char layer was expanded. However, the char layer formed by PP/IFR was not stable enough and continued to degrade at high temperatures. The total amount of alkanes and alkenes released by PP/IFR/CeO_2 were obviously lower than that of PP/IFR. Obviously, CeO_2 enhanced the structural integrity of the char layer, which blocked flammable gases such as alkanes inside. Therefore, the olefin produced by pyrolysis was carbonized.

3.3.5. Flame-retardant mechanism

Based on the above discussion, the flame retardancy mechanism is illustrated in Fig. 8. Pure PP burned rapidly when ignited, generating large amounts of toxic gases such as CO and CH_4, as well as dense smoke, and left no char residue after combustion. During combustion, APP decomposed to generate phosphoric acid and polyphosphoric acid.

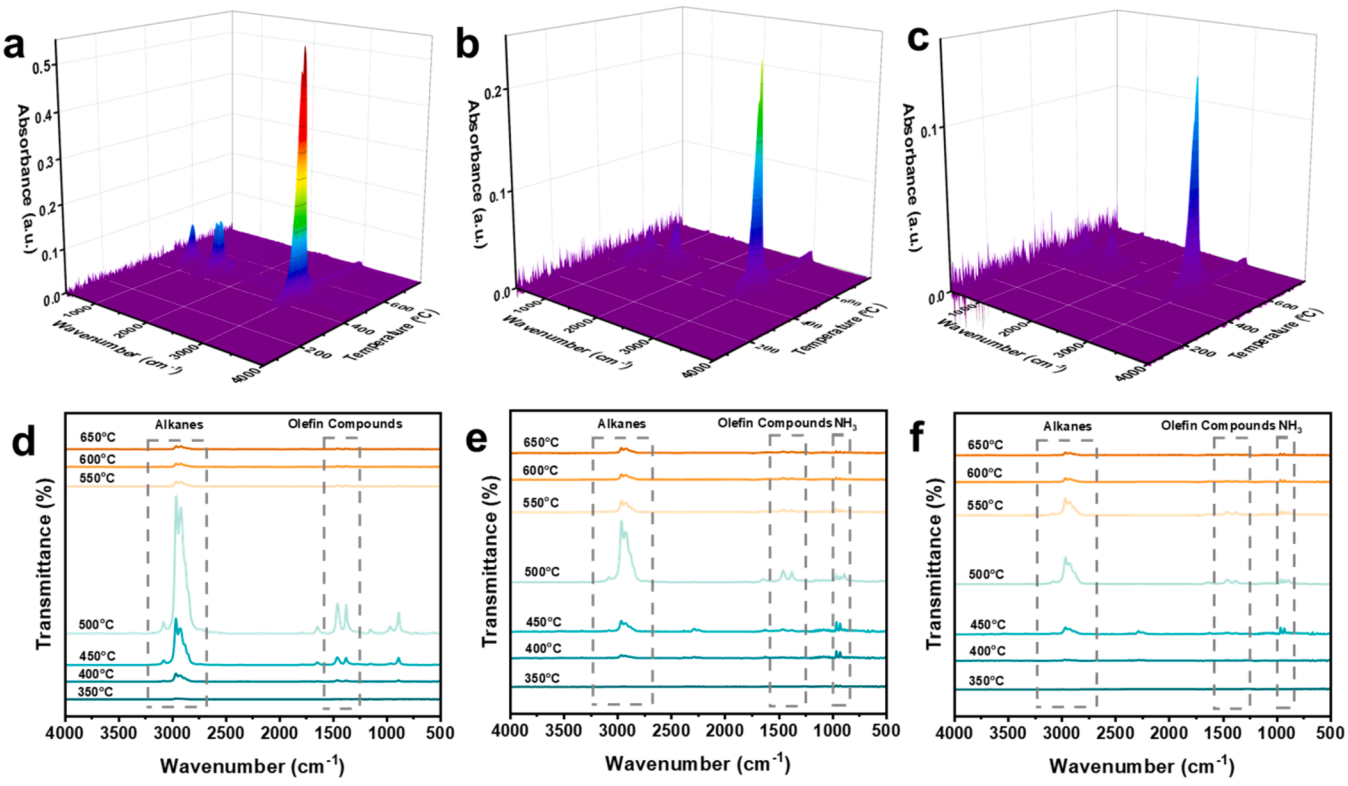

Fig. 7. 3D TG-IR spectra and IR spectra of pyrolysis products for (a, d) PP, (b, e) PP/IFR, and (c, f) PP/IFR/CeO_2.

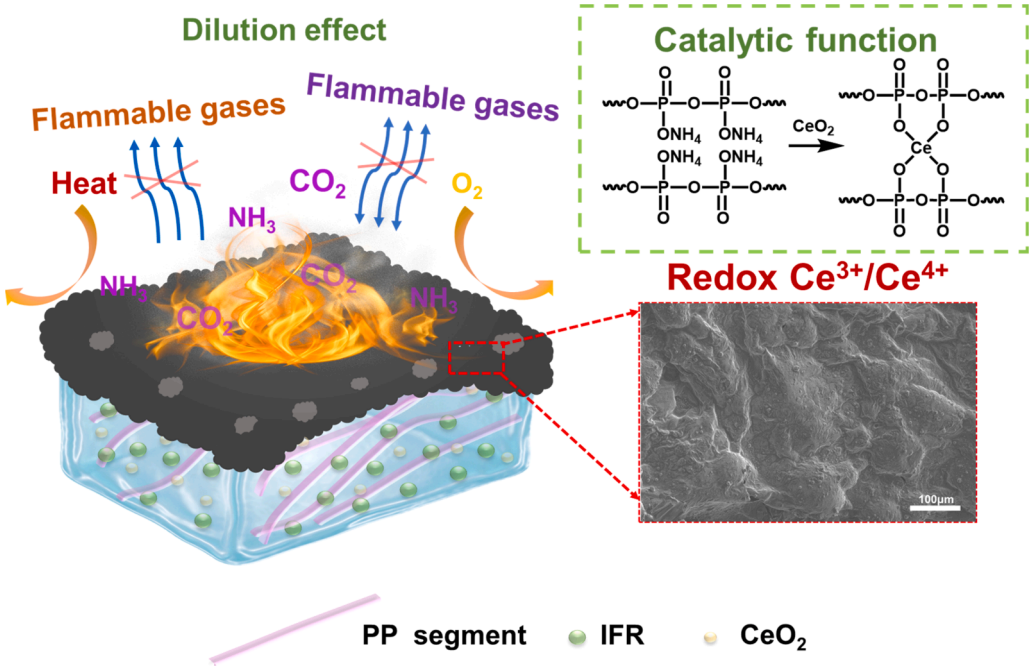

Fig. 8. Combustion mechanism of PP/IFR/CeO_2 composite.

Acting as effective catalysts, these generated acids promoted the dehydration and cross-linking of the polymer chains, thus facilitating the formation of a stable char layer. Concurrently, APP catalyzed CFA to produce inert gases (e.g., NH_3 and H_2O) under heating, providing adequate gas sources for dense expanded char layer formation. The resultant char layer effectively impeded oxygen and heat contact with the substrate, ultimately suppressing the combustion process. In addition, CeO_2 catalyzed the decomposition of combustible small molecules (e.g., hydrocarbons) produced during combustion into inert products such as CO_2 and NH_3, leveraging the reversible redox properties of Ce^{3+}/Ce^{4+}. Furthermore, CeO_2 functioned as an acid source, promoting esterification and dehydrogenation, which contributed to char formation [55]. These findings further demonstrate the catalytic role of CeO_2 in the thermal degradation process and the formation of dense, intumescent char layers is attributed to the synergistic effect between APP, CFA and CeO_2.

4. Conclusion

In this study, CeO_2 was combined with an intumescent flame retardant (IFR) to fabricate flame-retardant PP composites with enhanced UV aging resistance. Incorporating 20 wt% IFR/CeO_2 (mass ratio = 95: 5) enabled the PP/IFR/CeO_2 system to achieve a UL-94 V-0 classification with an LOI of 32.7 % because CeO_2 can collaborate with IFR to facilitate the formation of robust intumescent char layers on the PP matrix surface during combustion. In addition, the PP/IFR/CeO_2 system exhibited enhanced mechanical properties compared with PP/IFR system. After 120 h of UV exposure, the PP/IFR/CeO_2 sample exhibited a low CI value and effectively maintained its mechanical properties. Consequently, the PP/IFR/CeO_2 composite shows excellent UV aging resistance, flame retardancy, and mechanical performance. This study offers a viable, synergistic strategy for creating flame-retardant PP composites with extended durability.

CRediT authorship contribution statement

Jingqi Feng: Writing – original draft, Visualization, Investigation. **Ruiping Wang:** Writing – original draft, Investigation, Formal analysis. **Jiaqi Geng:** Validation. **Siqi Huo:** Writing – review & editing. **Zhiyong Zhang:** Formal analysis. **Miaojun Xu:** Supervision, Resources. **Mingyang Zhu:** Visualization. **Bin Li:** Supervision, Project administration.

Declaration of competing interest

The authors declare that they have no known competing financial interests or personal relationships that could have appeared to influence the work reported in this paper.

Acknowledge

This work was financially supported by the National Natural Science Foundation of China (52473071 and 52173069), the Key Research and Development Projects in Heilongjiang Province (2024ZXDXA29), and the Australian Research Council (DE230100616).

Supplementary materials

Supplementary material associated with this article can be found, in the online version, at doi:10.1016/j.polymdegradstab.2025.111850.

Data availability

Data will be made available on request.

References

[1] M.T. Hossain, M.A. Shahid, N. Mahmud, A. Habib, M.M. Rana, S.A. Khan, M. D. Hossain, Research and application of polypropylene: a review, Discover. Nano 19 (1) (2024) 2.
[2] Y. Guo, Q. Yang, S. Huo, J. Li, P. Jafari, Z. Fang, P. Song, H. Wang, Recyclable fire-retardant bio-based thermosets: from molecular engineering to performances and applications, Prog. Polym. Sci. 162 (2025) 101935.
[3] Y. Guo, N. Song, S. Huo, C. Wang, G. Ye, M. Hong, Y.T. Pan, T. Chen, Z. Chen, Y. Yu, P. Song, H. Wang, Strong, recyclable, bio-based vitrimers by tailored rigid-flexible structures for advanced carbon Fiber-reinforced polymers, Adv. Sci. (2025) e13935.
[4] S. Zhang, A.R. Horrocks, A review of flame retardant polypropylene fibres, Prog. Polym. Sci. 28 (11) (2003) 1517–1538.
[5] W. He, P. Song, B. Yu, Z. Fang, H. Wang, Flame retardant polymeric nanocomposites through the combination of nanomaterials and conventional flame retardants, Prog. Mater. Sci. 114 (2020) 100687.
[6] C. Wang, S. Huo, G. Ye, C.-F. Cao, M. Hong, Y.-T. Pan, P. Song, H. Wang, T. Wang, Z. Liu, Tick-inspired, self-healing, and strongly-adhesive coatings with biodegradability and phosphorus-free fire retardancy, J. Mater. Sci. Technol. 260 (2025) 229–240.
[7] C. Qu, Y. Wang, K. Yu, J. Zhao, Chemically modified copper tailings doped anti-UV aging coating for flame retarding plywood through catalytic charring, Constr. Build. Mater. 425 (2024) 135957.
[8] Y. Li, X. Chen, Q. Liu, J. Sun, H. Li, X. Gu, S. Jiang, S. Zhang, Constructing cross-functional intumescent flame retardants with UV resistance for polypropylene composites, Mater. Today Chem. 26 (2022) 101048.
[9] W. Brostow, X. Lu, O. Gencel, A.T. Osmanson, Effects of UV stabilizers on polypropylene outdoors, Materials 13 (7) (2020) 1626.
[10] R. Ma, M. Zhao, Y. Mo, P. Tang, Y. Feng, D. Li, HALS intercalated layered double hydroxides as an efficient light stabilizer for polypropylene, Appl. Clay Sci. 180 (2019) 105196.
[11] H. He, Q. Jiang, Y. Wan, M.H. Mia, X. Qu, M. Zhou, X. He, X. Li, M. Hong, Z. Yu, S. Huo, Biological skin-inspired damage warning and self-healing thermoelectric aerogel fiber via coaxial wet spinning for wearable temperature sensing, J. Mater. Sci. Technol. 250 (2026) 257–271.
[12] Y. Xu, S. Liang, W. Wang, C. Yan, L. Liu, D. Jiang, M. Hong, M. Xu, B. Li, S. Huo, Truss-inspired ultra-high strength, fire-safe, and thermal insulating double-crosslinked wood aerogels, J. Mater. Sci. Technol. 259 (2026) 268–278.
[13] N.S.S. Amorim, M. Nisar, G.M. Pinto, G.J.M. Fechine, Graphene oxide as an auxiliary UV photoprotector for polypropylene, Polym. Compos. (2025).
[14] X. Di, X. Chen, Y. Kang, J. Yang, Y. Zou, J. Jing, J. Sun, H. Li, X. Gu, S. Zhang, Introducing a polysiloxane coating on flame retardant to realize durable UV resistance and flame retardancy of polypropylene, Polym. Degrad. Stabil. 239 (2025) 111403.
[15] A.d.S.M. de Freitas, J.S. Rodrigues, V.R. Botaro, A.P. Lemes, S.A. Cruz, W. R. Waldman, Formation of craze-like pattern in polypropylene UV-induced surface cracking, J. Polym. Res. 29 (12) (2022) 506.
[16] X. Hu, Z. Sun, Z. Sun, Synthesis of a novel macromolecular carbon-nitrogen-phosphorous intumescent flame retardant, Adv. Powder Technol. 32 (5) (2021) 1341–1349.
[17] L. Han, W. Wu, Y. Qi, H. Qu, J. Xu, Synergistic flame retardant effect of $BiFeO_3$ in intumescent flame-retardant polypropylene composites, Polym. Compos. 38 (12) (2015) 2771–2778.
[18] Y. Sun, B. Yuan, S. Shang, H. Zhang, Y. Shi, B. Yu, C. Qi, H. Dong, X. Chen, X. Yang, Surface modification of ammonium polyphosphate by supramolecular assembly for enhancing fire safety properties of polypropylene, Compos. Part B-Eng. 181 (2020) 107588.
[19] L. Li, Y. Huang, W. Tang, Y. Zhang, L. Qian, Synergistic effect between piperazine pyrophosphate and melamine polyphosphate in flame retardant coatings for structural steel, Polymers 14 (18) (2022) 3722.
[20] H. Du, J. Ren, X. Fu, W. Zhang, R. Yang, Simultaneous improvements of the fire safety, mechanical properties and water resistance of vinyl ester resin composites by introducing microencapsulated ammonium polyphosphate by polytriazole, Compos. Part B-Eng. 238 (2022) 109908.
[21] W. Tang, L. Qian, Y. Chen, Y. Qiu, B. Xu, J. Li, Joint-aggregation intumescent flame-retardant effect of ammonium polyphosphate and charring agent in polypropylene, Polym. Adv. Technol. 31 (8) (2020) 1699–1708.
[22] L. Wu, Z. Mu, J. Lei, Z. Wei, J. Xing, X. Zhang, T. Jiang, X. Zeng, L. He, Foaming behavior, combustion behavior, and flame-retardant mechanism of PP/IFR/SiO_2 microcellular flame-retardant foams, Ind. Eng. Chem. Res. 64 (10) (2025) 5406–5416.
[23] S. Gao, Y. Li, Intumescent flame-retardant modification of polypropylene/carbon Fiber composites, J. Wuhan Univ. Technol., Mater. Sci. Ed. 37 (2) (2022) 163–169.
[24] Z. Zhao, Q. Jin, N. Zhang, X. Guo, H. Yan, Preparation of a novel polysiloxane and its synergistic effect with ammonium polyphosphate on the flame retardancy of polypropylene, Polym. Degrad. Stabil. 150 (2018) 73–85.
[25] K. Liu, Z. Wang, R. Pan, L. Xu, F. Zhu, Y. Zhang, Y. Meng, X. Xia, Double-layer microencapsulation of ammonium polyphosphate and its enhancement on the hydrophobicity and flame retardancy of cellulose paper, Int. J. Biol. Macromol. 284 (2025) 137924.
[26] X. Xiong, H. Shuang, C. Tao, L. Pingyang, D. Lingling, C. Yanhao, Properties and flame retarding mechanism of polypropylene with nitrogen-phosphorus flame retardant (Piperazine Polypyrophosphate) and its compound system, Polym. Mater. Sci. Eng. 36 (10) (2020) 71–78.
[27] S. Chen, B. Xiang, Y. Zhou, X. Zou, X. Lin, Functional triazine ultraviolet absorbers for sunlight protection of polymer materials surface, Mater. Lett. 236 (2019) 743–746.
[28] W. Zhao, C. Kundu, Z. Li, X. Li, Z. Zhang, Flame retardant treatments for polypropylene: strategies and recent advances, Compos. Part A-Appl. Sci. Manuf. 145 (2021) 106382.
[29] W. Zhao, Y. Cheng, Z. Li, X. Li, Z. Zhang, Improvement in fire-retardant properties of polypropylene filled with intumescent flame retardants, using flower-like nickel cobaltate as synergist, J. Mater. Sci. 56 (3) (2021) 2702–2716.
[30] X. Zheng, X. Chen, X. Guo, J. Sun, H. Li, X. Gu, S. Zhang, Tannic acid coated ammonium polyphosphate: for flame retardant and UV resistant of polypropylene, Polym. Degrad. Stabil. 229 (2024) 110956.
[31] Y. Li, B. Xue, S. Wang, J. Sun, H. Li, X. Gu, H. Wang, S. Zhang, Photoaging and fire performance of polypropylene containing melamine phosphate, ACS Appl. Polym. Mater. 2 (11) (2020) 4455–4463.
[32] K. An, C. Long, Y. Sui, Y. Qing, G. Zhao, Z. An, L. Wang, C. Liu, Large-scale preparation of superhydrophobic cerium dioxide nanocomposite coating with UV resistance, mechanical robustness, and anti-corrosion properties, Surf. Coat. Technol. 384 (2020) 125312.
[33] Y.W. Yao, K. Shi, J.J. Shang, Y.Y. Zhang, J.W. Lan, Mechanical, thermal, and ultraviolet resistance properties of polycarbonate/cerium oxide composites, Polym. Sci. Ser. A 58 (4) (2016) 578–584.
[34] L.W. Su, T.Y. Su, Z. Zhao, M.H. Liu, R.G. Xing, X. Ge, L.N. Jia, Y.H. Li, J.X. Bao, G. F. Pan, High-strength, flame-retardant, UV-resistant polyurethane elastomers

realized by synergizing nitrogen-phosphorus-containing ligands and cerium oxide nanoparticles, J. Appl. Polym. Sci. 142 (37) (2025) e57443.
[35] Y. Zhang, F. Lin, Y. Wu, S. Wang, Z. Liu, L. Song, Synergistic flame retardant effect of cerium-based DOPO derivative and intumescent flame retardants in polypropylene, J. Appl. Polym. Sci. 140 (18) (2023) e53819.
[36] W. He, F. Zhang, F. Zhang, Q. He, Effect of CeO_2 on UV aging of composite insulators prepared by template-spraying method, J. Appl. Polym. Sci. 140 (1) (2022) e53274.
[37] J. Hobson, G.-Z. Yin, X. Yu, X. Zhou, S.G. Prolongo, X. Ao, D.-Y. Wang, Synergistic effect of cerium oxide for improving the fire-retardant, mechanical and ultraviolet-blocking properties of EVA/magnesium hydroxide composites, Materials 15 (17) (2022) 5867.
[38] K. Yang, M.-J. Xu, B. Li, Synthesis of N-ethyl triazine-piperazine copolymer and flame retardancy and water resistance of intumescent flame retardant polypropylene, Polym. Degrad. Stabil. 98 (7) (2013) 1397–1406.
[39] M. Zhang, N. Liu, L. Hou, C. Li, C. Li, Adsorption behaviors of chlorpyrifos on UV aged microplastics, Mar. Pollut. Bull. 190 (2023) 114852.
[40] N.M. Ainali, D.N. Bikiaris, D.A. Lambropoulou, Aging effects on low-and high-density polyethylene, polypropylene and polystyrene under UV irradiation: An insight into decomposition mechanism by Py-GC/MS for microplastic analysis, J. Anal. Appl. Pyrolysis 158 (2021) 105207.
[41] B. Li, W. Hsu, T. Zheng, Y. Wu, S. Wang, F. Lin, L. Song, X. Rao, Morphology-engineered CeO_2 as a synergistic flame retardant in polypropylene/intumescent systems: mechanisms and performance enhancement, Molecules 30 (10) (2025) 2102.
[42] J. Bao, S.E. Ameyaw, Y. Gao, Z. Lu, W. Hu, Effect of ultraviolet aging on the structure and wear resistance of ultra-high-molecular-weight polyethylene ropes, Fibers Polym. 26 (6) (2025) 2305–2315.
[43] H.C. Han, X.L. Gong, M. Zhou, C. Li, H.B. Yang, A study about silane modification and interfacial ultraviolet aging of hemp fiber reinforced polypropylene composites, Polym. Compos. 42 (5) (2021) 2544–2555.
[44] Y. Li, B. Xue, P. Qi, X. Gu, J. Sun, H. Li, J. Lin, S. Zhang, The synergistic effect between bis (2,2,6,6-tetramethyl-4-piperidyl) sebacate and polysiloxane on the photo-aging resistance and flame retardancy of polypropylene, Compos. Part B-Eng. 234 (2022) 109666.
[45] Z. Liu, S. Xing, Y. Li, J. Sun, H. Li, X. Gu, S. Zhang, Surface modification of zinc oxide and its application in polypropylene with excellent fire performance and ultra-violet resistance, J. Colloid Interface Sci. 661 (2024) 307–316.
[46] X. Zhong, Y. Zhu, M. Jiang, Q. Sun, J. Yao, Photochemical synthesis of porous triazine-/heptazine-based carbon nitride homojunction for efficient overall water splitting, ChemSusChem 16 (8) (2023) e202202059.
[47] C. Cheng, S. Shuqian, S. Mingmei, W. Zhengwen, Z. Xingrong, T. Linsheng, Synergistic flame retardancy of ZnO with piperazine pyrophosphate/melamine polyphosphate in PP, Polym. Test. 117 (2023) 107878.
[48] Y. Xu, H. Hu, B. Tao, R. Yin, L. Liu, B. Li, Safe and economical preparation of amino acid-derived bio-based triazine char-forming agent for efficient intumescent flame retardant polypropylene, Constr. Build. Mater. 484 (2025) 141876.
[49] S. Li, W. Tang, L. Qian, J. Wang, X. Wu, Y. Qiu, W. Xi, In-suit cemented strategy enables intumescent flame retardant transition from hyper-hydrophilic to hydrophobic and aggregation flame retardant effect simultaneously in polypropylene, Compos. Part B-Eng. 287 (2024) 111874.
[50] Y. Lu, J. Feng, D. Yi, H. Xie, Z. Xu, C.F. Cao, S. Huo, H. Wang, P. Song, Strong synergistic effects between P/N-containing supramolecular microplates and aluminum diethylphosphinate for fire-retardant PA6, Compos. Part A-Appl. Sci. Manuf. 176 (2024) 107834.
[51] J. Liu, R. Wang, D. Liang, S. Zhang, J. Feng, M. Xu, S. Du, B. Li, Highly efficient polyethylene composites with flame-retardant, smoke and toxicity suppression properties by incorporating urchin-like ZnO@C-N and intumescent flame retardant, Polym. Degrad. Stabil. 233 (2025) 111190.
[52] E. Bèche, P. Charvin, D. Perarnau, S. Abanades, G. Flamant, Ce 3d XPS investigation of cerium oxides and mixed cerium oxide ($Ce_xTi_yO_z$), Surf. Interface Anal. 40 (3–4) (2008) 264–267.
[53] K.I. Maslakov, Y.A. Teterin, A.J. Popel, A.Y. Teterin, K.E. Ivanov, S.N. Kalmykov, V. G. Petrov, P.K. Petrov, I. Farnan, XPS study of ion irradiated and unirradiated CeO_2 bulk and thin film samples, Appl. Surf. Sci. 448 (2018) 154–162.
[54] Y. Wang, R. Guo, J. Zhang, H. Wang, B. Niu, H. Yan, P/N/Si-rich and flexible coating imparting polypropylene excellent flame retardancy without compromising its inherent mechanical properties, Chem. Eng. J. 487 (2024) 150519.
[55] T. Sai, S. Ran, S. Huo, Z. Guo, P. Song, Z. Fang, Sulfonated block ionomers enable transparent, fire-resistant, tough yet strong polycarbonate, Chem. Eng. J. 433 (2022) 133264.